Received: 7 February 2020 | Accepted: 9 April 2020

DOI: 10.1111/ina.12674

WILEY

ORIGINAL ARTICLE

Qualitative and quantitative schlieren optical measurement of the human thermal plume

Amayu W. Gena[1] | Conrad Voelker[1] | Gary S. Settles[2]

[1]Department of Building Physics, Bauhaus-Universität Weimar, Weimar, Germany

[2]Pennsylvania State University, University Park, PA, USA

Correspondence
Amayu W. Gena, Department of Building Physics, Bauhaus-Universität Weimar, Weimar, Germany.
Email: amayu.wakoya.gena@uni-weimar.de

Funding information
Deutscher Akademischer Austauschdienst (DAAD) Scholarship – Doctoral Programmes in Germany., Grant/Award Number: 57375975

Abstract

A new large-field, high-sensitivity, single-mirror coincident schlieren optical instrument has been installed at the Bauhaus-Universität Weimar for the purpose of indoor air research. Its performance is assessed by the non-intrusive measurement of the thermal plume of a heated manikin. The schlieren system produces excellent qualitative images of the manikin's thermal plume and also quantitative data, especially schlieren velocimetry of the plume's velocity field that is derived from the digital cross-correlation analysis of a large time sequence of schlieren images. The quantitative results are compared with thermistor and hot-wire anemometer data obtained at discrete points in the plume. Good agreement is obtained, once the differences between path-averaged schlieren data and planar anemometry data are reconciled.

KEYWORDS

digital image correlation, human thermal plume, schlieren imaging, schlieren velocimetry, thermal comfort, thermal manikin

1 | INTRODUCTION

In homogeneous media (solid, liquid, or gas), light propagates along straight lines as it travels at a constant velocity. But when media are inhomogeneous, the speed of light changes leading to a refraction of the light rays and a wavefront distortion. The inhomogeneities that refract light rays are known as *schlieren*, a German word meaning streaks. German physicist August Toepler (1836-1912) observed such small optical inhomogeneities in glass using an optical method that he named the schlieren technique.[1,2] Such refractions are sometimes visible with the naked eye (eg, mirages and the distortion of a background seen through antique window glass).

For the weak gradients of refractive index found in indoor air, a laboratory schlieren instrument using a precise concave mirror is has become the foremost visualization technique. In the 20th century, the schlieren technique became popular as a key tool of aerodynamics and wind tunnel testing, but it is also used in almost every branch of science and technology. In addition to Schardin,[2] modern references on the design and application of schlieren instruments include Merzkirch[3] and Settles.[4] A recent review including the influence of digital imaging and processing is given by Settles and Hargather.[5]

Specific to the fields of building and health science, schlieren optics is used for qualitative evaluation of the airflow supplied by personalized ventilation,[6] for investigation of the thermal plumes of human volunteers in a stratified environment for the improvement of an indoor environment,[7] to determine the dispersion and distribution characteristics of exhaled airflow for accurate prediction of disease transmission,[8,9] to demonstrate the importance of wearing a mask to reduce the potential for airborne transmission of infection over distance during human cough,[10] and to measure visible propagation distance during sneezing.[11]

The cited references took advantage of the characteristics of the schlieren technique: First, it requires only a rather simple optical arrangement. Second, it yields an easily interpreted image of

the refractive index gradient field at high resolution, making it ideal for flow visualization and especially for the study of indoor airflows. Third, the schlieren technique is non-intrusive; it does not require tracer particles as does particle image velocimetry (PIV), where particle seeding[12] can be challenging to control.

The Bauhaus-Universität Weimar thus decided to build its own large-scale schlieren optical system in 2018. It is intended for research projects in indoor airflow, such as the interaction of HVAC, the human thermal plume, and other sources of heat and contamination.[6,13-16] The setup also can be used for related areas of study such as acoustics, turbulence, and convective heat and mass transfer. It is one of a kind, especially due to the large 1-meter diameter of the schlieren mirror. This allows the imaging of large areas, which is necessary when investigating indoor airflow. Additionally, the specification of a concave spherical mirror with astronomical-quality surface accuracy allows the measurement of very weak air density gradients while requiring only one of the simplest of schlieren optical setups.

In this paper, this new schlieren system at Bauhaus-Universität Weimar is first introduced with a brief review of the mathematical principles involved. For the purpose of investigating the setup, an indoor air convective flow was measured and compared with the conventional thermal anemometry method. The thermal plume above a heated manikin serves as an example, which has been studied by the authors before,[14-16] but here schlieren velocimetry is performed by analyzing a large time sequence of schlieren images using digital cross-correlation software.

Practical implications

The findings of this study yield a qualitative and quantitative understanding of the human micro-environment. Additionally, the results of the new large-scale schlieren setup showed its capabilities to visualize convective indoor airflows with little density gradients. Thus, it inspires researchers to consider the schlieren method for the qualitative and quantitative analysis in various fields such as thermal comfort, HVAC, indoor air quality, building physics, and health science studies.

2 | MEASUREMENTS

2.1 | New schlieren imaging system

The schlieren optical system at Bauhaus-Universität Weimar is called a single-mirror coincident schlieren system, because it uses a single large spherical field mirror (Figures 1 and 2) and the light beams illuminating the mirror and forming an image in the camera are essentially coincident. The setup consists of four elements: (1) concave spherical mirror, (2) LED light source, (3) knife-edge schlieren cut-off, and (4) digital camera (Canon EOS 5DS R, with 50.6 megapixels image size and a 135 mm focal-length lens).

Because the setup is used for various indoor climate studies, a maximum flexibility of its arrangement was needed. Accordingly, the mirror is strap-mounted on an adjustable carriage. The carriage has four caster-type wheels (Item 5 in Figure 1), which makes it easy to reposition. For the purpose of leveling, the base frame of the carriage has three leveling bubbles (6) and four jackscrews (7) with hand wheels for precise leveling. A large hand wheel (8) is used to adjust the height of the mirror. Using the ruler (9) on the side of the lifting frame, it is possible to set the height of the center of the mirror to a desired value. The maximum adjustable height of the mirror center is about 2 m from the floor and the minimum is about 0.55 m. This degree of adjustability is unique and essential for the study of indoor climate scenarios.

With a diameter of 1 m, the mirror is among the largest schlieren mirrors in the world. To have a test area of 1 m diameter is important in order to accommodate a wide range of study samples in front of the mirror. By considering the available room size for installation of the system and the potential of installing it in a climate chamber, the focal length (f) of the mirror was chosen to be ~3 m, which requires a minimum of about a 9 m (the mirror radius of curvature, $R = 2f = 6$ m + 3 m standing area) long room.

The surface accuracy of the mirror is $\lambda/9.5$, where λ is the wavelength of HeNe laser light. This is considered as high precision grade or astronomical quality. This level of accuracy is needed for schlieren sensitivity, so that the weakest indoor airflows that refract light by less than one arcsecond can be seen against a uniform background without interference from flaws in the mirror figure. The mirror is

FIGURE 1 Schlieren imaging system at Bauhaus-Universität Weimar, see text for legend

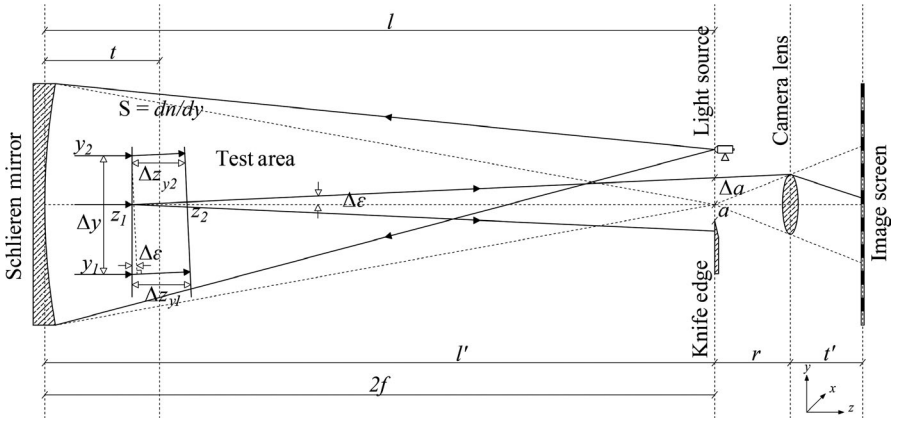

FIGURE 2 Diagram of single-mirror coincident schlieren imaging system (2f ≈ 6 m)

made from Astrositall glass-ceramic with a thickness/diameter ratio of 0.11. It is specified to have 2.7 nm RMS micro-roughness and a scratch/dig surface quality of 100/80.

In this setup, a light source is placed on the axis of the spherical mirror at its radius of curvature, $R = 2f$, as shown in Figure 2. After preliminary measurements, a small LED 2.1 × 2.1 × 0.27 mm in size with 284 lm luminous flux and 5000K color temperature was chosen as the best light source. The diverging light beam from the source fills the mirror and returns along the coincident path, crossing the thermal plume above the manikin at position (*l*–*t*). With coincident optics, each point in the schlieren object (S = d*n*/d*y*) is effectively traversed twice by the same light beam. To avoid double imaging, it is important to minimize the distance between the light source and the knife-edge, which is in this case only 5 mm.

Some rays are refracted as they enter the thermal plume of the manikin at z_1 in Figure 2. As a result of this refraction, these rays do not end up at the focal point assuming they have experienced a vertical refractive index gradient *dn/dy*. Those rays slightly refracted downwards by the angle $\Delta\varepsilon$ are blocked by the knife-edge. For this setup, the degree of knife-edge cutoff is set to be approximately 50%. While the blocked light rays create shadows in the schlieren image, the upward-refracted rays brighten the image. By these phenomena the flow features of the thermal plume are made visible. (A vertical refraction due to d*n*/d*y* and a horizontal knife-edge are assumed here for illustration purposes, but horizontal refractions due to d*n*/d*x* also occur, and require a vertical knife-edge to detect them.)

To capture such schlieren images, the camera was set manually to a shutter speed of 1/60 second, ISO 320, and lens aperture f/2. These settings were chosen to obtain high-quality single images with a correct exposure at a low light level in the room. To capture the convective heat release of the thermal manikin in motion, 0.92 megapixel schlieren images were captured at 50 frames/s for a 10 second interval (frame width 1280 pixels by 720 pixels in height).

2.1.1 | Mathematical model of the schlieren system

The underlying theory of the schlieren system is briefly described next, based on the Figure 2 and diagrams in refs.[3,4,17] The refraction of light rays depends on the indices of refraction of the schlieren object (S) and the surrounding undisturbed air. The refractive index *n* is defined as,

$$n = \frac{c_0}{c} \tag{1}$$

where c_0 is universal speed of light in vacuum, 3×10^8 m/s and *c* is the local light speed in a refractive medium. The *z*-axis of a right-handed Cartesian *x*,*y*,*z* coordinate system is the schlieren optical axis and also the direction of undisturbed rays approaching a zone of inhomogeneity. In Figure 2, the spherical wavefront of light is initially vertical upon passing from the left through z_1, but as it propagates through the schlieren object S to z_2, it covers the distance Δz in time Δt and is refracted through the small angle $\Delta\varepsilon$. Since light rays are always normal to their wavefronts, the ray passing though z_1 to z_2 is likewise refracted through $\Delta\varepsilon$. In Figure 2,

$$\Delta\varepsilon \approx \sin(\Delta\varepsilon) = \frac{\Delta z_{y1} - \Delta z_{y2}}{\Delta y} \tag{2}$$

then,

$$\Delta\varepsilon = \frac{(c_0/n_1) - (c_0/n_2)}{\Delta y}\Delta t \tag{3}$$

also,

$$\Delta t = \Delta z \frac{n}{c_0} \tag{4}$$

By combining Equations (3) and (4),

$$\Delta\varepsilon = \frac{n}{n_1 n_2}\frac{(n_1 - n_2)}{\Delta y}\Delta z \tag{5}$$

Which upon simplification yields

$$\frac{\partial\varepsilon}{\partial z} = \frac{1}{n}\frac{\partial n}{\partial y} \tag{6}$$

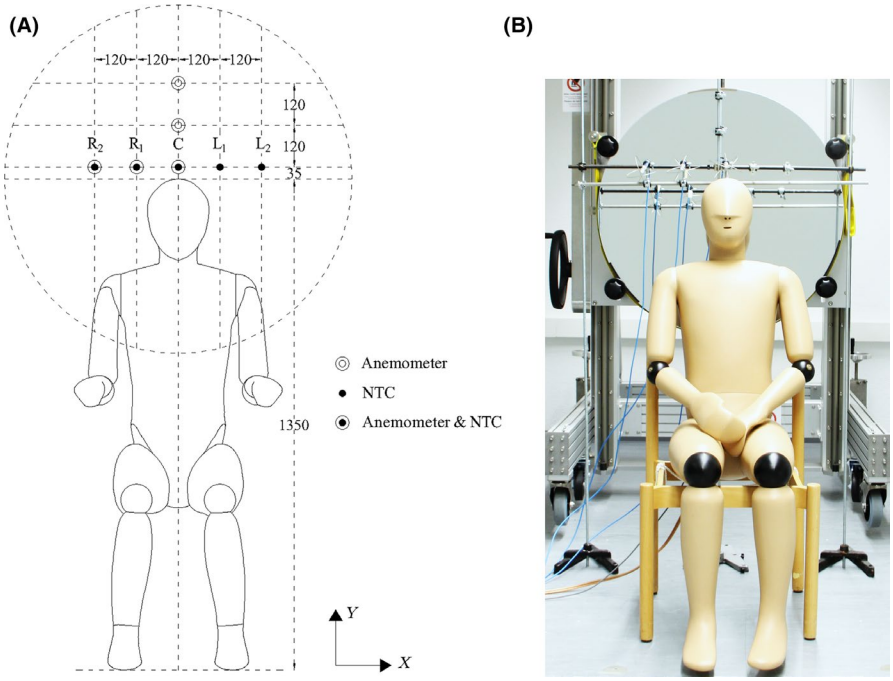

FIGURE 3 A, Technical drawing of the setup consisting of manikin, temperature sensors, and anemometers in front of the schlieren mirror, all the dimensions are in millimeter (mm). B, Photo of the same situation

But because ε is a very small angle, it is approximately equivalent to d*y*/d*z*, so the curvature of the refracted light ray in the *y*- and *x*-directions is given by

$$\frac{\partial^2 y}{\partial z^2} = \frac{1}{n}\frac{\partial n}{\partial y} \text{ and } \frac{\partial^2 x}{\partial z^2} = \frac{1}{n}\frac{\partial n}{\partial x} \tag{7}$$

By integrating these expressions, one obtains

$$\varepsilon_y = \frac{1}{n}\int \frac{\partial n}{\partial y}\,dz \text{ and } \varepsilon_x = \frac{1}{n}\int \frac{\partial n}{\partial x}\,dz \tag{8}$$

In summary, (a) refraction of light rays is caused by refractive index gradients ∂n/∂y and ∂n/∂x, (b) the refraction angles ε_y and ε_x are the result of the line-integrated influence of ∂n/∂y and ∂n/∂x across the test area from z_1 to z_2, and (c) light rays are always bent toward the region of higher *n*.

Also, in Figure 2 it is assumed that Δa is a shift of the light-source image as a consequence of $\Delta\varepsilon$, *a* is the height of the light source allowed to pass to camera aperture after cutoff at the knife-edge, $l = 2f$ is the distance from the schlieren mirror to the light source, $l' = 2f$ is the distance from schlieren mirror to knife-edge, and *t* is the distance from the schlieren mirror to the center of the schlieren object S. As a result,

$$\tan \Delta\varepsilon = \frac{\Delta a}{(l-t)} \tag{9}$$

and, as described in,[5] refraction angle $\Delta\varepsilon$ can be estimated by the thin-lens approximation of geometrical optics, where it is given approximately by:

$$\Delta\varepsilon = 2\left(n_s/n_a - 1\right) \tag{10}$$

where n_s is the refractive index at the pertinent point in schlieren object S, and n_a is the refractive index of the surrounding air. Using the above equations, the refraction angle $\Delta\varepsilon$ and the shift of the source image Δa can be calculated.

To test this mathematical model, measurements were carried out as described in Section 2.2. Note that the discussion of Figure 2 assumes a horizontal knife-edge detecting vertical beam deflections as shown in the figure. However, according to the same principles, a vertical knife-edge detecting horizontal gradients was used in the actual thermal plume measurements to be discussed later.

Finally, a simple linear relationship between the refractive index of a gas and its density ρ (Equation 11) and the perfect gas state equation (Equation 12) can be used to calculate n_s and n_a if ρ is known:

$$n - 1 = k\rho \tag{11}$$

where *k* is the Gladstone-Dale coefficient, which is ≈2.30×10^{-4} m^3/kg for air at standard conditions, and

$$\rho = P/RT \tag{12}$$

where *P* is absolute static pressure, *T* is absolute temperature, and *R* is the specific gas constant at 1 bar air pressure, *R* = 287.058 Pa·m^3/kg.

2.2 | Thermal manikin

To study the new schlieren system, the human thermal plume was investigated as an example. A thermal manikin (nicknamed "Feelix") was used to simulate heat release from the human body (Figure 3). The manikin has a complex male body shape that is 1.35 m high

in the upright sitting posture.[13,14] To simplify the measurements, the manikin is nude (without clothing or hair). According to Licina et al,[18] nudity results in higher convective flow velocities compared to cases using dressed manikins with hair. Since flow imaging and measurement are the aims of this paper, this is a desirable result.

To simplify the measurements, a wooden chair frame served as a seat. Also, the manikin's breathing was turned off. Its surface temperature was manually set to 34°C to simulate that of the human skin, with a precision of ±0.2°C according to refs.[13,19]

To avoid accidental contact with the sensitive mirror, the thermal manikin was placed not directly in front of the mirror but approximately 0.6 m forward of it at the center. The elevation of the manikin's crown is 1.35 m above the floor, while the center of the mirror is positioned at 1.25 m (the same height as the optical axis including light source, knife-edge, and camera).

2.3 | Thermal anemometry and thermistors

To validate the air velocity of the manikin's thermal plume, to be analyzed by cross-correlation algorithm from schlieren imaging in chapter 3.3, measurement of air velocity using thermal anemometers was carried out. Five Ahlborn hot-wire omni-directional anemometers with ±1.5% accuracy (according to the manufacturer) were used. Of the five, three were placed on a line at 3.5 cm above the manikin's crown on the C, R1, and R2 axes shown in Figure 3. The results of the anemometer R1 and R2 were mirrored to the L1 and L2, assuming the air velocity fields above the right and the left shoulders of the manikin are similar since the shoulders themselves are similar. The other two anemometers were placed on the vertical C axis at 15.5 and 27.5 cm above manikin's crown. The anemometer measurements were recorded over a time period t = 30 minutes with a sampling interval of t = 1 seconds and were then averaged. During these measurements, there were no sources of natural or forced convection in the room other than the manikin and the experimenter, who remained far from the test area. Therefore, the air velocity in the room tended to be almost 0 m/s which was indicated by an anemometer measurement.

To measure the temperature of the thermal manikin plume, five Ahlborn's negative-temperature-coefficient thermistors (NTC) with an accuracy of ±0.1 K (according to the manufacturer) were used. These thermistors were placed on a line at 3.5 cm above manikin's crown on the R2, R1, C, L1, and L2 axes (Figure 3) and used to measure the manikin's thermal plume over time t = 30 minutes with sampling interval of t = 2 seconds. Additionally, the air temperature of the surrounding undisturbed indoor climate room was measured in parallel. Due to the large dimensions of the room and the resulting large capacity, the only heat source therein (the manikin) had almost no impact on the room air temperature, resulting in a constant room air temperature ($\theta_{\text{room air}}$) of 25°C. Also, all other heat sources and the ventilation system in the room were turned off. The NTC thermistor measurements were used to analyze the refractive index of the thermal plume ($n_{\text{thermal plume}}$) and the room air ($n_{\text{room air}}$), as described in chapter 3.2.

FIGURE 4 Example vertical-knife-edge schlieren image from the 500-image ensemble used for thermal plume analysis

3 | RESULTS AND DISCUSSIONS

3.1 | Schlieren image analysis

The schlieren image in Figure 4 shows the flow of the thermal plume of the seated naked manikin due to buoyancy. It also illustrates the resulting light refraction and its visualization via the schlieren technique. Based on schlieren image observation, laminar to transitional airflow is visible above the shoulders of the manikin and near the arms. Above the manikin's head, however, turbulent flow is observed once the plume has fully separated from the manikin. The roughly estimated Reynolds number for airflow just above the manikin's head is between 4.6×10^3 and 7.4×10^3 at a plume velocity between 0.15 and 0.24 m/s, based on the anemometer measurements. For this estimate, a 50 cm shoulder width and a 34°C surface temperature of the manikin with 25°C room air temperature were used.

During schlieren image acquisition, the vertically oriented knife-edge blocked the source image from the left side. As a result, dark-shaded features are visible on the left side of the plume and contrasting bright features of the flow are visible from the right, which is opposite the knife-edge. Since the flow is highly transient, the schlieren image of Figure 4 is only an instantaneous snapshot. A long sequence of these images will be used to estimate the displacement of the flow features as a function of time using digital image correlation in chapter 3.3.

3.2 | Refractive index analysis

Schlieren images like Figure 4 can be used not only to visualize the flow, but also to perform quantitative measurements of the air

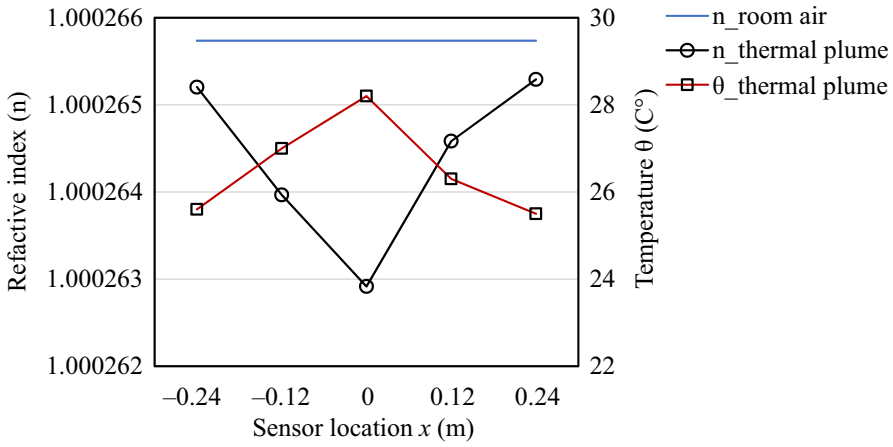

FIGURE 5 Refractive index profile of thermal plume, refractive index of room air, and average plume temperature profile at 3.5 cm above manikin's crown

density and temperature under certain conditions. A key assumption is that thermal convection is a constant-pressure process, the local pressure P being measured by a barometer or inferred from atmospheric data and the local height above sea level. The perfect gas state equation (Equation 12) then relates air temperature T and density ρ, from which ρ can be found using the presently measured plume temperature profile, T. Then the Gladstone-Dale relation (Equation 11) provides the corresponding profile of refractive index n, as shown in Figure 5. Also Equation 9 provides an estimate of the refraction angle $\Delta\varepsilon$ and the resulting shift of the light-source image Δa in the knife-edge plane, as shown in Figure 6.

Figure 5 shows higher temperatures in the middle and lower ones at the edge of the plume. As a result, the refractive index, which is inversely proportional to temperature, is lower at the middle and higher at the sides, as is the air density. Since the room air temperature ($\theta_{\text{room air}}$) was uniform at 25°C, its refractive index ($n_{\text{room air}}$) is likewise uniform. Also, in the center of the plume there is a high refractive index difference between the plume and the room air, and a smaller difference at the sides.

From Figure 6, there is a small refraction angle $\Delta\varepsilon$ and hence a small shift of the source image Δa near the edges of the plume but a peak in these parameters directly over the manikin's crown. Δa is observed to be quite small, at most about 30 μm, and $\Delta\varepsilon$ <2 arcseconds. Similar values were found from schlieren images of convection from a human hand by Schardin[2] (reproduced by Settles[4]).

The present measurements of Δa and $\Delta\varepsilon$ are only average values, however, because the line-integral nature of Equation 8 yields averages across the plume in the z-direction, not values at specific z coordinates.

Bearing this in mind, Table 1 tabulates these results as a function of sensor location. Collectively, these results demonstrate the high sensitivity of the present 1-meter-aperture schlieren system and its value for indoor climate studies.

3.3 | Displacement analysis

To analyze the 500-frame time sequence of schlieren photos quantitatively and qualitatively, the open-source software PIVlab[20] has been used. Originally, PIVlab was developed for digital particle image velocimetry (DPIV), calculating the particle displacement by evaluating the cross-correlation of many small sub-images (interrogation windows) between two PIV images, image A at t_o and image B at $t_o + \Delta t$.[21] Hence, the velocity magnitudes between image A and image B can be derived from Δt and the distance that the particles travelled between images (particle displacement). However, PIVlab is capable of processing other types of pattern displacement than just PIV particle images.

Cross-correlation is a statistical technique that assesses pattern similarity between interrogation window A and shifted interrogation

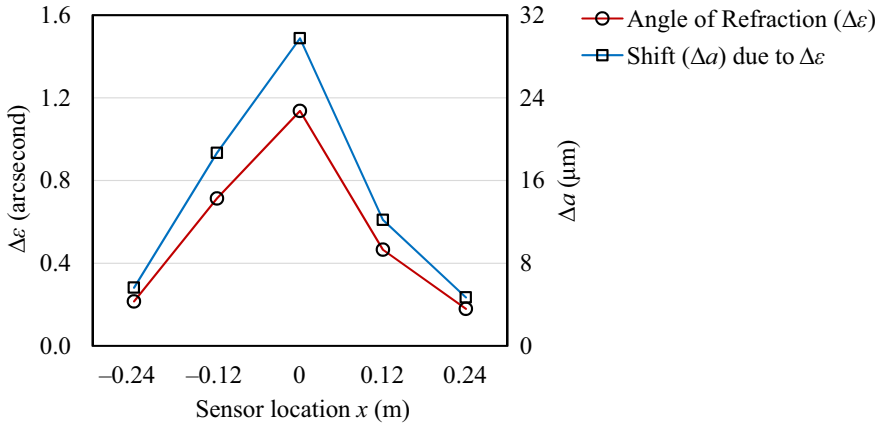

FIGURE 6 Estimated refraction angle $\Delta\varepsilon$ and light-source-image shift Δa, at each sensor location 3.5 cm above the manikin's crown

TABLE 1 Measured values vs. location from the refractive index analysis

Sensor location	Δε (arcsecond)	Δ*a* (μm)	Δ*T* (K)	Δε/Δ*T*	Δ*a*/Δ*T*
R_2	0.21	5.62	0.6	0.358	9.379
R_1	0.71	18.67	2	0.356	9.336
C	1.14	29.76	3.2	0.355	9.3
L_1	0.47	12.18	1.3	0.358	9.375
L_2	0.18	4.69	0.5	0.358	9.381

window B. This statistical technique is applied using a discrete cross-correlation function[12,20]

$$C(x,y) = \sum_i \sum_j A(i,j)B(i+x,j+y) \quad (13)$$

where *C*(*x*, y) is the cross-correlation coefficient and *A* and *B* are corresponding interrogation window areas from image A and image B. Higher cross-correlation coefficient values represent the best match between images, thus yielding their displacement values.

PIVlab is programmed in MATLAB and requires the MATLAB Image Processing Toolbox to run. It consists of three main steps: image pre-processing, image analysis, and post-processing. For this analysis, 500 consecutive schlieren images were used as input to assess the displacement between each image pair, yielding 250 vector displacement fields.

As an example, Figure 7A depicts the manikin in front of the schlieren mirror. The manikin and the surroundings have been masked, as they are not a part of the flow analysis. In the background, the schlieren image of the rising airflow remains visible. The green vectors added by the cross-correlation algorithm comparing images 1 and 2 of a single pair indicate the displacements of the flow features (in pixels) which are stored as a gray value. In some regions (eg, above the manikin's left shoulder) no vectors appear because, at this location, the flow is laminar with no moving structures to correlate. Outside the plume altogether, flow velocities are very low and again there is little to correlate, so only "noise" vectors appear. (These are usually removed deliberately in PIVlab post-processing.)

To have a more reliable result than Figure 7A, averaging all 250 vector fields was necessary. PIVlab's interpolation approach[21] was used to average the 250 vector fields into a single mean vector field shown in Figure 7B. Obviously a much smoother mean result is obtained this way than in Figure 7A. Missing vectors in Figure 7A are replaced by interpolated data, and outliers are manually filtered out by placing limits on acceptable velocities in post-processing. The mean vector field of Figure 7B was therefore used for data extraction.

PIVlab offers several possibilities for data extraction from a vector field, including using paths (as in Figure 8) or areas. The data can also be exported as a colormap (Figure 9), movies, or images (Figure 7). The detailed workflow of DPIV analysis in PIVlab can be found in ref.[21]

To compare the results of the anemometer experiments and PIVlab-derived measurements, the locations of NTC thermistors and anemometers during the experiments (see Figure 3) were traced onto the mean vector field image of Figure 7B. Moreover, the location at 3.5 cm above manikin's crown, which was used for refractive index analysis due to its higher ΔT between $\theta_{\text{room air}}$ and $\theta_{\text{thermal plume}}$, was also examined for a detailed displacement analysis as shown in Figures 10 and 11. Thus, the velocity magnitude of the manikin's thermal plume at similar locations with the anemometers at 3.5, 15.5, and 27.5 cm above the crown was extracted from the mean schlieren displacement vector field (Figure 7B) and plotted in Figure 8.

Figure 8 shows that the maximum measured upward air velocity above the manikin's crown is about 0.16 m/s measured at 15.5 cm above the crown. Beyond that the centerline velocity of the thermal plume deceases so that, at 27.5 cm, the maximum velocity is only slightly above 0.12m/s. The black curve (at 27.5 cm) and the red curve (at 15.5 cm) are peaked and relatively smooth but not so in the case of blue curve (at 3.5 cm). Nevertheless, the shapes of the three

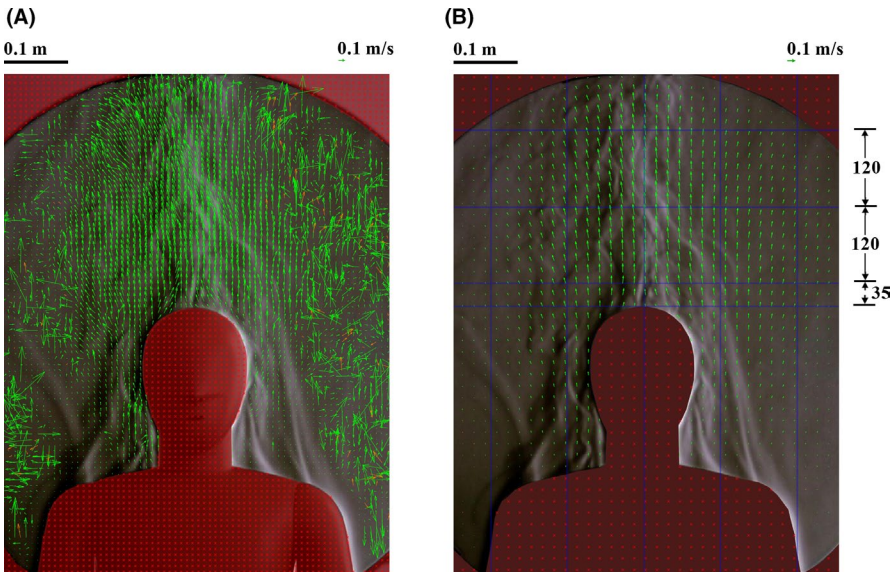

FIGURE 7 PIVlab cross-correlation analysis, (A) vector field generated from images 1 and 2 only, (B) mean vector field of 250 image pairs from 500 schlieren images, the dimensions are in mm. For clarity, fewer but larger vectors are shown in (B) than (A)

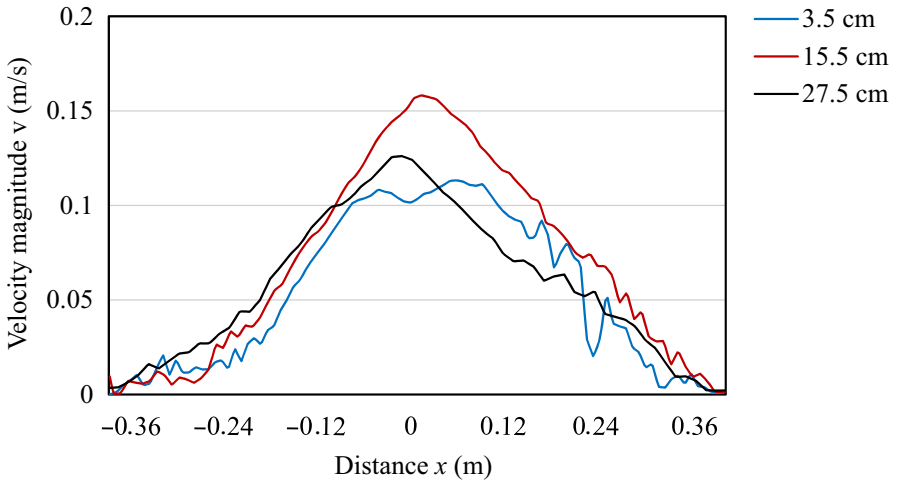

FIGURE 8 Velocity magnitude of the manikin's thermal plume at different heights above the crown, extracted from the mean vector field (Figure 7B)

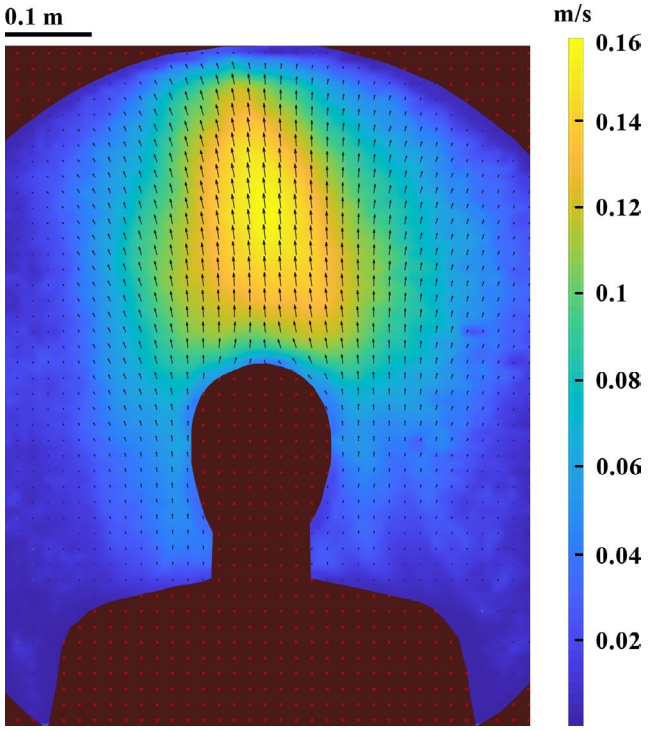

FIGURE 9 PIVlab velocity colormap showing the velocity magnitude of the manikin's thermal plume with vector overlay and color bar

curves are generally similar and represent the expected bell shape of a thermal plume velocity profile.

Figure 9 shows the velocity colormap of interpolated mean vector field with a color bar more clearly than just with vectors. It can be seen that the velocity increases with distance above the manikin's crown, reaches its measured maximum of 0.16 m/s, and then decreases with additional height. The figure also shows a small "dead zone" directly above the head, as noted in a previous study by Voelker et al using particle streak tracking.[15]

For a detailed analysis of the results from the cross-correlation of schlieren images, the velocity magnitude of the thermal plume at 3.5 cm above the manikin's crown was further investigated. As shown in Figure 10, the shape of the velocity profile from the mean vector field and the error bars of the 250 data sets agree around the center of the plume, within ~0.12 m on either side of x = 0. The error bars show the standard deviation of the 250 schlieren data sets. The error bars on the left side are relatively larger, signaling a growing inaccuracy as the velocity magnitude decreases nearer the edges of the plume. In contrast, the velocity magnitude from the mean vector field does not obviously lose accuracy with distance from x = 0 and is in good agreement with a superposed Gaussian curve shown in red. (The mean velocity profiles of axisymmetric plumes and jets are known to be Gaussian beyond a sufficient distance from their origins[22,23]).

It remains to compare the PIVlab mean-velocity-profile measurements with the hot-wire anemometer measurements made in a vertical plane passing through the crown of the manikin's head. The schlieren image is definitely not a plane-section measurement like PIV[12] or the present anemometer data, but rather is the line-integral of light rays that have crossed the entire flowfield, as already described. So, the schlieren data are the result of flow features that are path-averaged in depth along the z-axis across the thermal plume of the manikin. On the face of it, this is not a fair comparison, but since something is to be learned from it, the two results are compared in Figure 11.

Figure 11 shows the anemometer data including its standard deviation error bars and the schlieren image-correlation data already shown in earlier figures, both at 3.5 cm above manikin's crown. The anemometer data have the same Gaussian profile shape but twice the centerline velocity of the schlieren results. This disagreement is not unexpected and is due to the fact that the anemometer data are planar centerline data while the schlieren data are path-averaged across the entire plume.

Insight into this can be gained from published studies of schlieren image-correlation velocimetry applied to fully developed axisymmetric turbulent jets.[5,24] The jet case is analogous to, but simpler than, the present one because it is axisymmetric (two dimensional), has Gaussian velocity profiles when fully developed, and has an established scaling law for centerline velocity as a function of downstream distance from the jet origin. PIV

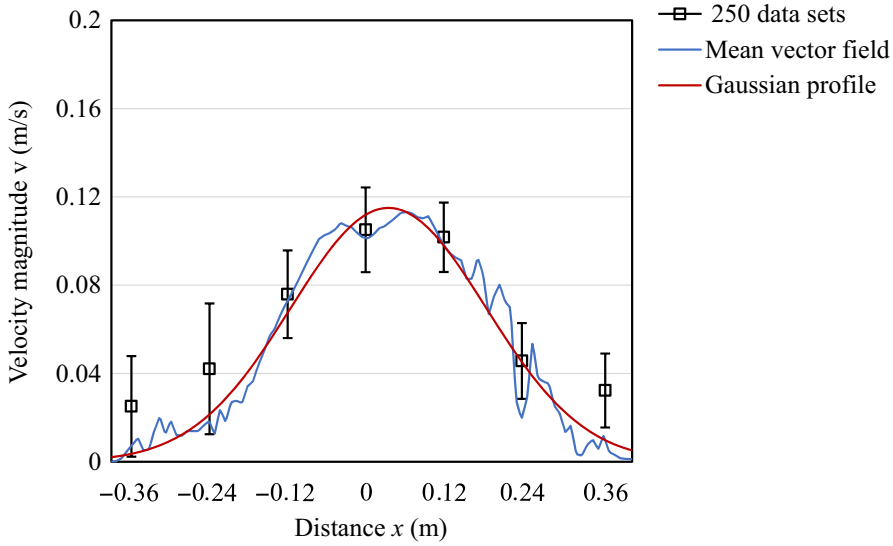

FIGURE 10 A closer examination of the thermal plume velocity profile extracted from 250 schlieren image pairs using PIVlab at 3.5 cm above the manikin's crown

and schlieren image-correlation data were compared by Jonassen et al,[24] who found that the latter underpredicted the former by a factor of two. This was ascribed to the effect of the forward Abel transform in projecting the axisymmetric jet structure onto a plane. They referred to their approach as "schlieren image velocimetry" (later just *schlieren velocimetry*). Settles and Hargather[5] further noted that the forward Abel transform of an axisymmetric Gaussian profile is also Gaussian, so the only remaining question concerns the ratio of transformed to original centerline velocities. That question is somewhat clouded by uncertainty about whether the available experimental data actually support the assumption of a Gaussian profile near the outer edge of a jet or plume, but it is now clear that schlieren velocimetry, when applied to turbulent plumes and jets, can be relied upon to predict a centerline velocity of about half the value measured by true planar instruments like PIV or centerline anemometer arrays. Also, of relevance, recent work by Schmidt et al[25] has taken a critical look at schlieren velocimetry and rendered advice on when it can and cannot be properly applied.

4 | CONCLUSION

Schlieren images can be used not only to visualize the flow, but also to perform quantitative measurements of the air density and temperature under certain conditions. The Gladstone-Dale relation (Equation 11) and Equation 9 can be used to estimate the refractive index n, the refraction angle $\Delta\varepsilon$, and the resulting shift of the light-source image Δa in the knife-edge plane. As a result, Δa around 30 μm and $\Delta\varepsilon$ less than 2 arcseconds are observed. These results demonstrate the high sensitivity of the Bauhaus-Universität Weimar schlieren system and its value for indoor climate studies.

PIVlab can be used to process schlieren images. Large time sequence of schlieren images (eg, 500 pairs) is enough to provide good

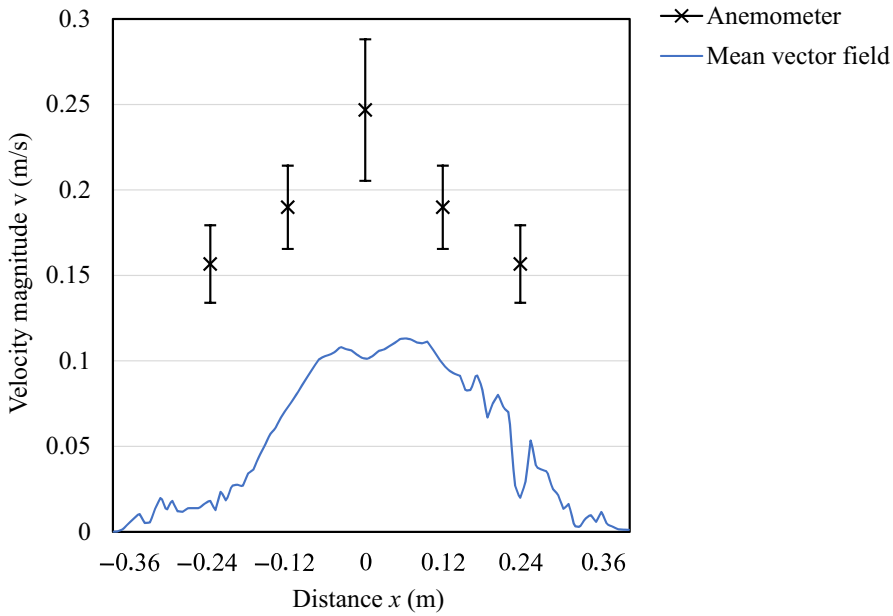

FIGURE 11 Investigation of thermal plume using schlieren velocimetry data and anemometers at 3.5 cm above manikin's crown

average of flow velocities in the manikin's plume. However, PIVlab requires turbulent flow and cannot succeed for laminar flow and when the flow velocities are very low.

Even though the anemometer data are planar centerline data while the schlieren data are path-averaged across the entire plume, the extracted data from mean vector field of the schlieren images and the anemometer data have the same Gaussian profile shape but anemometer data is twice the centerline velocity of the schlieren results. In general, the schlieren velocimetry, when applied to turbulent plumes and jets, can be relied upon to predict a centerline velocity of about half the value measured by true planar instruments like PIV or centerline anemometer arrays.

Moreover, while it explains the velocity discrepancy in Figure 11, the analogy between the manikin's plume and axisymmetric turbulent jets is only approximate because the plume is not very axisymmetric. A more thorough approach would involve tomographic imaging of the manikin's upper-body flow and plume over an angular range of 180° in, say, 10° increments, followed by 3D image reconstruction using inverse Radon transform software and filtered back projection, for example.[26] This is certainly possible with the schlieren instrument described here, but is well outside the scope of the present paper.

Finally, until recently, the schlieren technique was regarded as essentially qualitative compared first to laser holographic interferometry, then laser-Doppler anemometry, and now PIV. Digital imaging and digital image processing have changed that view.[5] Schlieren is now seen as a direct source of high-quality flow imaging at high data rates, amenable to a variety of digital analysis codes yielding quantitative data. Examples of this are already found in aerospace, combustion, and fundamental fluid dynamics research, but indoor air, building physics, and health science still mostly await making use of this new capability.

ACKNOWLEDGEMENT

The authors are grateful to the German Academic Exchange Service (DAAD) for their support.

ORCID

Amayu W. Gena https://orcid.org/0000-0002-0812-3801
Conrad Voelker https://orcid.org/0000-0002-3687-0177

REFERENCES

1. Toepler A. *Beobachtungen nach einer neuen optischen Methode: Ein Beitrag zur experimental-Physik*. Bonn: Max Cohen & Sohn; 1864:50.
2. Hubert S. Die Schlierenverfahren und ihre Anwendungen. *Ergebnisse der Exakten Naturwissenschaften*. 1942;20:303-439.
3. Merzkirch W. *Flow Visualization* (2nd edn.). Orlando: Academic Press; 1987:260.
4. Settles G. *Schlieren and Shadowgraph Techniques*. Berlin, Heidelberg: Springer; 2001:376.
5. Settles GS, Hargather MJ. A review of recent developments in schlieren and shadowgraph techniques. *Meas Sci Technol*. 2017;28:42001.
6. Alsaad H, Voelker C. Qualitative evaluation of the flow supplied by personalized ventilation using schlieren imaging and thermography. *Build Environ*. 2020;167:106450.
7. Craven BA, Settles GS. A computational and experimental investigation of the human thermal plume. *Fluids Eng*. 2006;128:1251-1258.
8. Xu C, Nielsen PV, Liu L, Jensen RL, Gong G. Human exhalation characterization with the aid of schlieren imaging technique. *Build Environ*. 2017;112:190-199.
9. Tang JW, Noakes CJ, Nielsen PV, et al. Observing and quantifying airflows in the infection control of aerosol- and airborne-transmitted diseases: an overview of approaches. *J Hospital Infect*. 2011;77:213-222.
10. Tang JW, Liebner TJ, Craven BA, Settles GS. A schlieren optical study of the human cough with and without wearing masks for aerosol infection control. *J R Soc Interface*. 2009;6:727-736.
11. Tang JW, Nicolle AD, Klettner CA, Pantelic J, Wang L, Suhaimi AB. Airflow dynamics of human jets. *PLoS ONE*. 2013;8:60-67.
12. Raffel M. *Particle Image Velocimetry: A Practical Guide* (3rd edn). Cham: Springer; 2018:669.
13. Alsaad H, Voelker C. Performance assessment of a ductless personalized ventilation system using a validated CFD model. *J Building Perf Simul*. 2018;11:689-704.
14. Voelker C, Alsaad H. Simulating the human body's microclimate using automatic coupling of CFD and an advanced thermoregulation model. *Indoor Air*. 2018;28:415-425.
15. Voelker C, Maempel S, Kornadt O. Measuring the human body's microclimate using a thermal manikin. *Indoor Air*. 2014;24:567-579.
16. Gena AW. Schlieren imaging and analysis. 30. *Forum Bauinformatik*. 2018;323-330.
17. Weinstein LM. Review and update of lens and grid schlieren and motion camera schlieren. *Eur Phys J Special Topics*. 2010;182:65-95.
18. Licina D, Pantelic J, Melikov A, Sekhar C, Tham KW. Experimental investigation of the human convective boundary layer in a quiescent indoor environment. *Build Environ*. 2014;75:79-91.
19. Tanabe S, Arens EA, Bauman F, Zhang H, Madsen T. Evaluating thermal environments by using a thermal manikin with controlled skin surface temperature. *ASHRAE Transact*. 1994;100:39-48.
20. Thielicke W, Stamhuis EJ. PIVlab – towards user-friendly, affordable and accurate digital particle image velocimetry in MATLAB. *Open Res Software*. 2014;2:1202-1212.
21. Willert CE, Gharib M. Digital particle image velocimetry. *Exp Fluids*. 1991;10:181-193.
22. Turner JS. *Buoyancy Effects in Fluids*. Cambridge, UK: Cambridge University Press; 2012:382 p.
23. Pope SB. *Turbulent Flows*. Cambridge, UK: Cambridge University Press; 2000:796 p.
24. Jonassen DR, Settles GS, Tronosky MD. Schlieren "PIV" for turbulent flows. *Opt Lasers Eng*. 2006;44:190-207.
25. Schmidt BE, Page WE, Sutton JA. Seedless velocimetry in a turbulent jet using schlieren imaging and a wavelet-based optical flow method. *AIAA Scitech*. 2020;Forum:2020–2207.
26. Clackdoyle R, Defrise M. Tomographic reconstruction in the 21st century. *IEEE Signal Process Mag*. 2010;27:60-80.

How to cite this article: Gena AW, Voelker C, Settles GS. Qualitative and quantitative schlieren optical measurement of the human thermal plume. *Indoor Air*. 2020;30:757–766. https://doi.org/10.1111/ina.12674